JACS
JOURNAL OF THE AMERICAN CHEMICAL SOCIETY
Communication
pubs.acs.org/JACS

Nanoscale Metal–Organic Framework for Highly Effective Photodynamic Therapy of Resistant Head and Neck Cancer

Kuangda Lu,[†] Chunbai He,[†] and Wenbin Lin*

Department of Chemistry, University of Chicago, 929 East 57th Street, Chicago, Illinois 60637, United States

Supporting Information

ABSTRACT: Photodynamic therapy (PDT) is an effective anticancer procedure that relies on tumor localization of a photosensitizer followed by light activation to generate cytotoxic reactive oxygen species (e.g., $^1O_2$). Here we report the rational design of a Hf–porphyrin nanoscale metal–organic framework, DBP–UiO, as an exceptionally effective photosensitizer for PDT of resistant head and neck cancer. DBP–UiO efficiently generates $^1O_2$ owing to site isolation of porphyrin ligands, enhanced intersystem crossing by heavy Hf centers, and facile $^1O_2$ diffusion through porous DBP–UiO nanoplates. Consequently, DBP–UiO displayed greatly enhanced PDT efficacy both *in vitro* and *in vivo*, leading to complete tumor eradication in half of the mice receiving a single DBP–UiO dose and a single light exposure. NMOFs thus represent a new class of highly potent PDT agents and hold great promise in treating resistant cancers in the clinic.

Photodynamic therapy (PDT) is a phototherapy that combines three nontoxic components, a photosensitizer (PS), a light source, and tissue oxygen, to cause toxicity to malignant and other diseased cells.[1] The mechanism of PDT involves energy transfer from the light-excited PS to oxygen and other molecules in the tissue to generate reactive oxygen species (ROS), particularly, singlet oxygen ($^1O_2$), which induces cellular toxicity.[1,2] PDT can lead to localized destruction of diseased tissues via selective uptake of the PS and/or local exposure to light, providing a minimally invasive cancer therapy. The application of PDT in cancer treatment dates back to 1970s when hematoporphyrin derivatives were studied for PDT efficacy *in vivo*,[1] and the first PDT agent photofrin was approved for clinical use in 1993. Most clinically used PSs are from the porphyrin family, with a few other dyes emerging as efficient PSs in recent years.[3]

Selective localization of PSs in tumors is critical for effective PDT. However, many PSs are hydrophobic in nature, which not only leads to insufficient tumor localization but also causes PS aggregation to diminish the PDT efficacy.[4] Significant synthetic modifications are thus needed to render these PSs effective PDT agents *in vivo*. An alternative approach is to use nanocarriers to selectively deliver therapeutic or PDT agents to tumors via the enhanced permeation and retention (EPR) effect and some times via active tumor targeting with ligands that bind to overexpressed receptors in cancers.[4,5] Indeed, a number of nanoparticle platforms have been developed to deliver molecule- or material-based PDT and photothermal agents to cancers; and in some cases, encouraging clinical data are emerging.[6]

Nanoscale metal–organic frameworks (NMOFs), constructed from metal ion/ion clusters and organic bridging ligands, have recently emerged as a promising nanocarrier platform for therapeutic and imaging agents.[7] Compared to other nanocarriers, NMOFs combine many beneficial features into a single delivery platform, including tunable chemical compositions and crystalline structures; high porosity; and biodegradability. For example, we used a NMOF to deliver both cisplatin (in the pores) and siRNAs (on the surface) to overcome drug resistance in ovarian cancer,[7j] and more recently, we demonstrated real-time intracellular pH sensing in live cells with a fluorescent NMOF by taking advantage of its crystalline and porous structure.[8]

Here we report the design of a Hf–porphyrin NMOF as a highly effective PS for PDT of resistant head and neck cancer. Although porphyrin-based MOFs have been intensively studied,[9] the delivery of PDT agents using porphyrin-based NMOFs has not been realized. We hypothesized that the incorporation of a porphyrin-derived bridging ligand into a robust and porous UiO NMOF structure with proper morphologies and dimensions would have several advantages over existing nanoparticle PDT agents: first, the PS molecules are well-isolated in the framework to avoid aggregation and self-quenching of the excited states; second, coordination of porphyrin ligands to heavy Hf centers via the carboxylate groups can promote intersystem crossing to enhance ROS generation efficiency; third, the porous NMOF structure provides a pathway for facile diffusion of ROS (such as $^1O_2$) out of the NMOF interior to exert their cytotoxic effects on cancer cells. In this NMOF design, an unprecedentedly high PS loading can be achieved to enable highly effective PDT of difficult-to-treat cancers.

The new porphyrin derivative, 5,15-di(*p*-benzoato)porphyrin (H_2DBP), was synthesized by a condensation reaction between 4-(methoxycarbonyl)benzaldehyde and dipyrrylmethane, and characterized by ^{1}H and ^{13}C NMR spectroscopy and mass spectrometry (Figures S3–S5, Supporting Information [SI]). The linearly aligned dicarboxylate groups of the DBP ligand allow the construction of a DBP–UiO NMOF with the framework formula of $Hf_6(\mu_3\text{-}O)_4(\mu_3\text{-}OH)_4(DBP)_6$. DBP–UiO was synthesized by a solvothermal reaction between $HfCl_4$ and H_2DBP in *N*,*N*-dimethylformamide (DMF) at 80 °C (Scheme 1). The resulting dark purple powder was washed with copious amounts of DMF, 1% triethylamine in ethanol (v/

Received: August 22, 2014
Published: November 19, 2014

   dx.doi.org/10.1021/ja508679h | *J. Am. Chem. Soc.* 2014, 136, 16712–16715

Scheme 1. Synthesis of Hf–DBP NMOF and the Schematic Description of Singlet Oxygen Generation Process

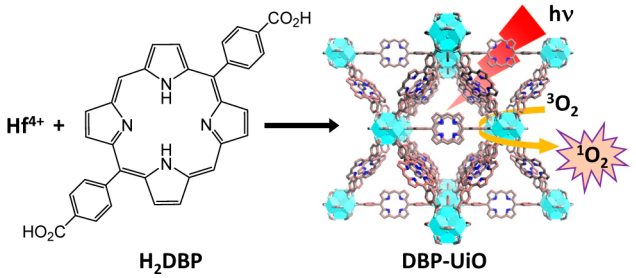

v), and ethanol successively before being dispersed in ethanol as a stock suspension.

Numerous attempts failed to grow DBP–UiO crystals suitable for single-crystal X-ray diffraction. Fortunately, we have determined the single crystal structure of an analogue of DBP–UiO, $Zr_6(\mu_3\text{-}O)_4(\mu_3\text{-}OH)_4(Zn\text{–}DPDBP)_6$ (Zn–DPDBP–UiO, DPDBP is 5,15-di(*p*-benzoato)-10,20-diphenylporphyrin and has the same length as DBP; Table S1 and Figure S6, SI), whose powder X-ray diffraction (PXRD) pattern is essentially the same as that of DBP–UiO (Figure 1a). DBP–UiO thus adopts a UiO-type MOF structure that is built from 12-connected $Hf_6(\mu_3\text{-}O)_4(\mu_3\text{-}OH)_4$ secondary building units (SBUs) and DBP bridging ligands.[10] DBP–UiO has a very open framework structure with triangular channels of 1.6 nm in dimensions as well as octahedral and tetrahedral cavities of 2.8 and 2.0 nm in dimensions, respectively.

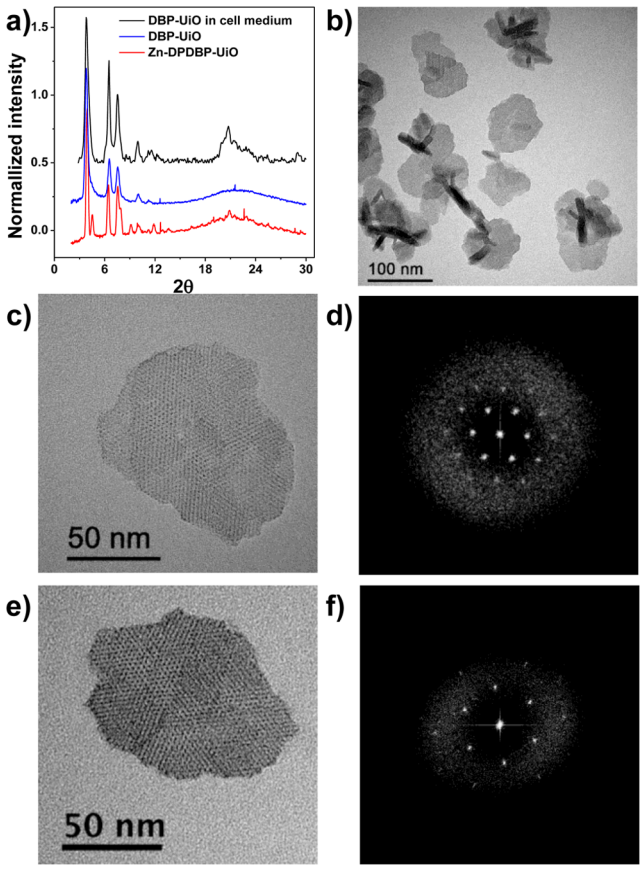

Figure 1. Morphology and structure of DBP–UiO. (a) PXRD patterns of Zn–DPDBP–UiO, DBP–UiO, and DBP–UiO after incubating in RPMI 1640 cell culture medium for 12 h. (b) TEM image of DBP–UiO showing nanoplate morphology; high-resolution TEM images of DBP–UiO samples before (c) and after (e) cell-medium cultivation, and their fast Fourier transform patterns (d,f), respectively.

DBP–UiO particles display a plate morphology by transmission electron microscopy (TEM) (Figure 1b and Figure S7, SI). Nitrogen adsorption measurements gave a BET surface area of 558 m^2/g for DBP–UiO (Figure S8, SI). The composition of DBP–UiO was confirmed by thermogravimetric analysis (Figure S9, SI) and inductively coupled plasma–mass spectrometry (ICP–MS), giving DBP loading of 77 wt % (calcd 73%) and Hf content of 24.3% (calcd 23.7%), respectively. These results also indicate that DBP ligands do not coordinate to Hf^{4+} ions via nitrogen atoms during the UiO synthesis (the Hf content would have been 37.2% if all DBP ligands were metalated).

Individual SBUs are clearly visible in high-resolution TEM images of DBP–UiO (Figure 1c). The distances between SBUs are measured to be approximately 2.7 nm (Figure S10, SI), which are consistent with the calculated distances of 2.77 nm based on the X-ray structure model. Fast Fourier transform (FFT) of the high-resolution TEM image displays a 3-fold symmetry for the nanoplates (Figure 1d), consistent with the cubic crystal system of the DBP–UiO. The dimensions of the nanoplates are measured to be ~100 nm in diameter and ~10 nm in thickness. Such thin plates consist of only 4–5 sets of (111) packing layer (d_{111} = 2.2 nm). Dynamic light scattering (DLS) measurements gave an average diameter of 76.3 nm for the particles (Figure S11, SI). Notably, the nanoplate morphology is particularly advantageous for generating ROS for PDT. The diffusion length of $^1O_2$ is no more than 90–120 nm in aqueous environment[11] and was estimated to be 20–220 nm inside cells.[12] Therefore, the nanoplates as thin as 10 nm in thickness are ideally suited for transporting $^1O_2$ from the NMOF interior to the cell cytoplasm to exert cytotoxic effects.

The UiO framework was recently shown to be stable in aqueous solution.[7j,10] DBP–UiO was incubated in RPMI 1640 cell culture medium for 12 h to determine its stability in physiologically relevant media. TEM images showed an unaltered morphology of the nanoplates, and FFT proved that the crystalline structure of DBP–UiO remained intact (Figures 1e,f and S12, SI). The PXRD patterns of the NMOF samples before and after incubation in RPMI 1640 medium are identical (Figure 1a), further confirming structural stability of DBP–UiO in physiological environments.

The UV–visible absorption spectra of H_2DBP and DBP–UiO in phosphate buffer saline (PBS) buffers (pH = 7.4) are compared in Figure 2a. H_2DBP shows a Soret band at 402 nm and four Q-bands at 505, 540, 566, and 619 nm. The extinction coefficients of H_2DBP at 402 and 619 nm are 2.2×10^5 and 1.7×10^3 M^{-1} cm^{-1}, respectively (Figures S13 and 14, SI). DBP–UiO shows slight red shifts for all Q-bands, with the peaks appearing at 510, 544, 579, and 634 nm. The red-shifts probably result from the coordination of the carboxylate groups of DBP ligands to Hf^{4+} centers. The presence of four Q-bands and their red shifts further support the presence of free-base porphyrin ligands in DBP–UiO. The Soret band of DBP–UiO is significantly broadened, presumably due to inequivalent ligand environments in thin nanoplates as well as potential framework distortion in thin MOF structures.

Singlet oxygen generation efficiencies of H_2DBP and DBP–UiO were determined using Singlet Oxygen Sensor Green (SOSG, Life Technologies). After exposure to a LED light source (peak emission at 640 nm and energy irradiance of 100 mW/

dx.doi.org/10.1021/ja508679h | J. Am. Chem. Soc. 2014, 136, 16712–16715

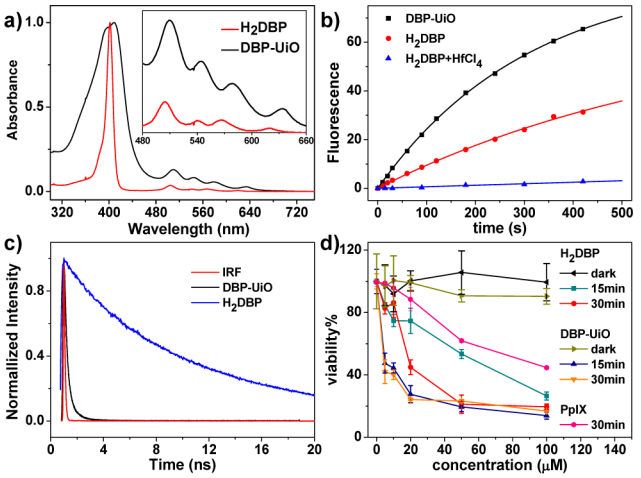

Figure 2. (a) Absorption spectra of H_2DBP and DBP−UiO in PBS. (b) Singlet oxygen generation by DBP−UiO, H_2DBP, and H_2DBP + $HfCl_4$. The dots are experimental data and the solid lines are fitted curves. (c) Time-resolved fluorescent decay traces of H_2DBP and DBP−UiO along with instrument response function (IRF). (d) *In vitro* PDT cytotoxicity of H_2DBP, DBP−UiO, and PpIX at different PS concentrations and irradiation times.

cm^2; Figure S17, SI), the chemiluminescent reagent SOSG reacted with $^1O_2$ to generate green fluorescence, which was quantified with a fluorimeter. The fluorescence intensity was plotted against irradiation time (Figure 2b). The $^1O_2$ generation was depicted with an exponential function that corresponded to a pseudo first-order process. The $^1O_2$ generation curve was fitted with the following equation:

$$I_F = A(1 - e^{-kt}) \quad (1)$$

where I_F is fluorescence intensity and t represents irradiation time, while A and k are fitting parameters (for detailed derivations, see SI). The fitted equations for H_2DBP and DBP−UiO are (Table S3, SI)

$$I_{H2DBP} = 68 \times (1 - e^{-0.0015t}) \quad (2)$$

$$I_{DBP-UiO} = 88 \times (1 - e^{-0.0033t}) \quad (3)$$

The product of Ak in the equation is proportional to the initial rate of the reaction that indicates the $^1O_2$ generation efficiency (see discussion in SI). DBP−UiO is thus at least twice as efficient as H_2DBP in generating $^1O_2$, presumably owing to heavy Hf^{4+} centers facilitating the intersystem crossing from the ^{1}DBP to ^{3}DBP excite state.[13] Consistent with this, the ^{1}DBP emission intensity at 640 nm greatly diminished for DBP−UiO (by a factor of ∼250; Figure S15, SI) with a lifetime reduction from 10.9 ns for H_2DBP to 0.26 ns for DBP−UiO (Figures 2c and S16 and Table S2, SI). As a control, addition of Hf^{4+} to the H_2DBP ligand solution did not enhance but rather reduce the generation of $^1O_2$ (Figure 2b).

Encouraged by the excellent $^1O_2$ generation efficiency, we tested the PDT efficacy of DBP−UiO on resistant head and neck cancer. Head and neck cancer refers to a group of biologically similar cancers that arise in the head or neck region (including nasal cavity, sinuses, lips, mouth, salivary glands, throat, and larynx). Current treatments of head and neck cancers include surgery and radiation therapy, with chemotherapy and chemo-radiotherapy playing some roles.[14] Since head and neck cancers occur superficially, PDT represents a viable alternative treatment modality.[15]

In vitro PDT was performed on human head and neck cancer cells SQ20B, which are resistant to cisplatin and radiation therapy. The tumor cell uptake of DBP−UiO was first evaluated by incubating SQ20B cells with DBP−UiO (30 μg/mL) for 4 or 12 h (Figure S20, SI). The Hf concentrations in the cells were determined by ICP−MS. No significant difference was observed between the cells after 4 and 12 h incubations, showing rapid internalization of DBP−UiO by cancer cells.

To further confirm the PDT efficacy of DBP−UiO, SQ20B cancer cells were treated with H_2DBP, DBP−UiO, or protoporphyrin IX (PpIX) at various concentrations (5, 10, 20, 50, and 100 μM based on ligand concentrations), and the cells were irradiated with LED light (640 nm, 100 mW/cm^2) for 15 min (total light dose 90 J/cm^2) or 30 min (total light dose 180 J/cm^2), respectively. Significant PDT efficacy was observed in DBP−UiO treated groups, even for the group receiving 5 μM PS dose and 15 min irradiation (Figure 2d). H_2DBP-treated groups show moderate PDT efficacy only at 20 μM dose with 30 min light irradiation, while no cytotoxicity was observed in dark control or blank control groups. In comparison, PpIX is much less photocytotoxic than DBP−UiO under similar conditions (Figure 2d).

We carried out proof-of-concept *in vivo* experiments on SQ20B subcutaneous xenograft murine models to evaluate the PDT efficacy of DBP−UiO. The mice were treated with PBS control, DBP−UiO (3.5 mg DBP/kg), or H_2DBP (3.5 mg/kg) by intratumoral injection. Twelve hours post injection, each mouse was irradiated at the tumor site with light (180 J/cm^2) for 30 min. For comparison, photofrin is administrated by intraperitoneal injection at 10 mg/kg in tumor bearing mice and with light irradiation of 135 J/cm^2.[16] As depicted in Figure 3a, the tumors of mice treated with DBP−UiO started shrinking 1 day post DBP−UiO administration and PDT. Most importantly, among the four tumors in the DBP−UiO group, two tumors were completely eradicated by single DBP−UiO administration and single light irradiation, while the sizes of the

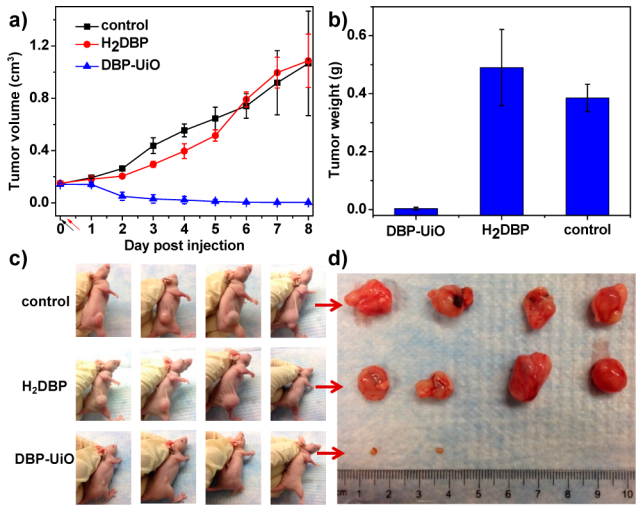

Figure 3. *In vivo* efficacy of PDT on SQ20B tumor bearing mice. (a) Tumor growth inhibition curve after PDT treatment. Black and red arrows refer to injection and irradiation time points, respectively. (b) Tumor weight after PDT treatment. (c) Photos of the mice on Day 8. (d) Photo of tumors of each group after PDT. Two tumors in the DBP−UiO group were completely eradicated at the end point.

dx.doi.org/10.1021/ja508679h | J. Am. Chem. Soc. 2014, 136, 16712−16715

other two tumors decreased from ~150 to ~3 mm^3 (Figure 3b–d). The tumor growth of mice treated with H_2DBP was slightly suppressed after PDT, however, accelerated after 5 days and exhibited no difference to the control group at the end point. After local administration, DBP–UiO could be efficiently internalized by the tumor cells and induce cytotoxicity upon irradiation, while the free ligand might be cleared away from the tumor sites before irradiation. No skin/tissue damage was observed after PDT treatment on all mice (Figure 3c). Histologies of tumor slices showed macrophage infiltration in tumors of the DBP–UiO treated group and indicated that significant fractions of tumor cells were undergoing apoptosis/necrosis (Figure S21, SI).

In summary, we have designed and synthesized a stable and porous DBP–UiO NMOF with an ideal combination of structural regularity and nanoplate morphology for highly effective PDT of resistant head and neck cancer. As a result of site isolation of DBP ligands, enhanced intersystem crossing by Hf clusters, and facile $^1O_2$ diffusion out of a porous nanoplate, the NMOF works as an efficient PDT photosensitizer, as demonstrated by both $^1O_2$ generation efficiency measurements and *in vitro* cytotoxicity assays. *In vivo* PDT efficacy studies with subcutaneous xenograft murine models demonstrated 50 times tumor volume reduction in half of the mice and complete tumor eradication in the other half of the mice that were treated with DBP–UiO. In comparison, no therapeutic effect was observed in the mice treated with H_2DBP. The facile structural and compositional tunability of NMOFs should allow further tuning of other properties to afford a new generation of highly potent PDT agents for treating resistant cancers in the clinic.

■ ASSOCIATED CONTENT

Supporting Information

Experimental details for the synthesis and characterization of H_2DBP, DBP–UiO, and Zn–DPDBP–UiO, photochemical properties and singlet oxygen generation, cellular uptake, and *in vitro* and *in vivo* efficacy studies. This material is available free of charge via the Internet at http://pubs.acs.org.

■ AUTHOR INFORMATION

Corresponding Author

*wenbinlin@uchicago.edu

Author Contributions

†These authors contributed equally to this work.

Notes

The authors declare no competing financial interest.

■ ACKNOWLEDGMENTS

We acknowledge NIH (UO1-CA151455) for funding support. We thank Dr. Cheng Wang, Teng Zhang, Zekai Lin, Christopher Poon, Carter Abney, and Seth Barrett for experimental help. We acknowledge the use of the Biophysical Dynamics NanoBiology Facility, which is partially funded by NIH Grant 1S10RR026988-01.

■ REFERENCES

(1) Dolmans, D. E. J. G. J.; Fukumura, D.; Jain, R. K. *Nat. Rev. Cancer* **2003**, *3*, 380–387.

(2) Pass, H. I. *J. Natl. Cancer Inst.* **1993**, *85*, 443–456.

(3) Allison, R. R.; Sibata, C. H. *Photodiagn. Photodyn.* **2010**, *7*, 61–75.

(4) Bechet, D.; Couleaud, P.; Frochot, C.; Viriot, M.-L.; Guillemin, F.; Barberi-Heyob, M. *Trends Biotechnol.* **2008**, *26*, 612–621.

(5) (a) Wang, A. Z.; Langer, R.; Farokhzad, O. C. *Annu. Rev. Med.* **2012**, *63*, 185–198. (b) Maeda, H.; Sawa, T.; Konno, T. *J. Controlled Release* **2001**, *74*, 47–61. (c) Fang, J.; Nakamura, H.; Maeda, H. *Adv. Drug Delivery Rev.* **2011**, *63*, 136–151.

(6) (a) Lovell, J. F.; Jin, C. S.; Huynh, E.; Jin, H.; Kim, C.; Rubinstein, J. L.; Chan, W. C.; Cao, W.; Wang, L. V.; Zheng, G. *Nat. Mater.* **2011**, *10*, 324. (b) Jin, C. S.; Cui, L.; Wang, F.; Chen, J.; Zheng, G. *Adv. Healthcare Mater.* **2014**, *3*, 1240–1249. (c) Samia, A. C.; Chen, X.; Burda, C. *J. Am. Chem. Soc.* **2003**, *125*, 15736–15737. (d) Cheng, Y.; Doane, T. L.; Chuang, C. H.; Ziady, A.; Burda, C. *Small* **2014**, *10*, 1799–1804. (e) Cobley, C. M.; Chen, J.; Cho, E. C.; Wang, L. V.; Xia, Y. *Chem. Soc. Rev.* **2011**, *40*, 44–56. (f) Chen, J.; Wang, D.; Xi, J.; Au, L.; Siekkinen, A.; Warsen, A.; Li, Z.-Y.; Zhang, H.; Xia, Y.; Li, X. *Nano Lett.* **2007**, *7*, 1318. (g) Wang, Y.; Black, K. C.; Luehmann, H.; Li, W.; Zhang, Y.; Cai, X.; Wan, D.; Liu, S.-Y.; Li, M.; Kim, P. *ACS Nano* **2013**, *7*, 2068. (h) Loo, C.; Lowery, A.; Halas, N.; West, J.; Drezek, R. *Nano Lett.* **2005**, *5*, 709–711. (i) Lal, S.; Clare, S. E.; Halas, N. J. *Acc. Chem. Res.* **2008**, *41*, 1842–1851. (j) Kumar, R.; Roy, I.; Ohulchanskky, T. Y.; Vathy, L. A.; Bergey, E. J.; Sajjad, M.; Prasad, P. N. *ACS Nano* **2010**, *4*, 699–708. (k) Carter, K. A.; Shao, S.; Hoopes, M. I.; Luo, D.; Ahsan, B.; Grigoryants, V. M.; Huang, H.; Zhang, G.; Pandey, R. K. *Nat. Commun.* **2014**, *5*, 3546.

(7) (a) Tranchemontagne, D. J.; Mendoza-Cortes, J. L.; O'Keeffe, M.; Yaghi, O. M. *Chem. Soc. Rev.* **2009**, *38*, 1257–1283. (b) Spokoyny, A. M.; Kim, D.; Sumrein, A.; Mirkin, C. A. *Chem. Soc. Rev.* **2009**, *38*, 1218–1227. (c) Rieter, W. J.; Taylor, K. M.; An, H.; Lin, W. *J. Am. Chem. Soc.* **2006**, *128*, 9024–5. (d) Rieter, W. J.; Pott, K. M.; Taylor, K. M. L.; Lin, W. *J. Am. Chem. Soc.* **2008**, *130*, 11584–11585. (e) deKrafft, K. E.; Xie, Z.; Cao, G.; Tran, S.; Ma, L.; Zhou, O. Z.; Lin, W. *Angew. Chem., Int. Ed.* **2009**, *48*, 9901–4. (f) Taylor-Pashow, K. M.; Della Rocca, J.; Xie, Z.; Tran, S.; Lin, W. *J. Am. Chem. Soc.* **2009**, *131*, 14261–3. (g) Horcajada, P.; Chalati, T.; Serre, C.; Gillet, B.; Sebrie, C.; Baati, T.; Eubank, J. F.; Heurtaux, D.; Clayette, P.; Kreuz, C.; Chang, J.-S.; Hwang, Y. K.; Marsaud, V.; Bories, P.-N.; Cynober, L.; Gil, S.; Ferey, G.; Couvreur, P.; Gref, R. *Nat. Mater.* **2010**, *9*, 172. (h) Della Rocca, J.; Liu, D.; Lin, W. *Acc. Chem. Res.* **2011**, *44*, 957–968. (i) Liu, D.; Huxford, R. C.; Lin, W. *Angew. Chem., Int. Ed.* **2011**, *50*, 3696–3700. (j) He, C.; Lu, K.; Liu, D.; Lin, W. *J. Am. Chem. Soc.* **2014**, *136*, 5181–5184. (k) Morris, W.; Briley, W. E.; Auyeung, E.; Cabezas, M. D.; Mirkin, C. A. *J. Am. Chem. Soc.* **2014**, *136*, 7261–7264.

(8) He, C.; Lu, K.; Lin, W. *J. Am. Chem. Soc.* **2014**, *136*, 12253–12256.

(9) (a) Gao, W.-Y.; Chrzanowski, M.; Ma, S. *Chem. Soc. Rev.* **2014**, *43*, 5841–5866. (b) Lee, D. H.; Kim, S.; Hyun, M. Y.; Hong, J. Y.; Huh, S.; Kim, C.; Lee, S. J. *Chem. Commun.* **2012**, *48*, 5512–5514. (c) Feng, D.; Gu, Z. Y.; Li, J. R.; Jiang, H. L.; Wei, Z.; Zhou, H. C. *Angew. Chem., Int. Ed.* **2012**, *124*, 10453–10456. (d) Zhang, M.; Gu, Z.-Y.; Bosch, M.; Perry, Z.; Zhou, H.-C. *Coord. Chem. Rev.* **2014**, DOI: 10.1016/j.ccr.2014.05.031.

(10) Cavka, J. H.; Jakobsen, S.; Olsbye, U.; Guillou, N.; Lamberti, C.; Bordiga, S.; Lillerud, K. P. *J. Am. Chem. Soc.* **2008**, *130*, 13850–13851.

(11) (a) Kanofsky, J. R. *Photochem. Photobiol.* **2011**, *87*, 14–17. (b) Stdenis, C. E.; Fell, C. J. D. *Can. J. Chem. Eng.* **1971**, *49*, 885. (c) Merkel, P. B.; Kearns, D. R. *J. Am. Chem. Soc.* **1972**, *94*, 7244–7253. (d) Rodgers, M. A. J.; Snowden, P. T. *J. Am. Chem. Soc.* **1982**, *104*, 5541–5543. (e) Snyder, J. W.; Skovsen, E.; Lambert, J. D. C.; Ogilby, P. R. *J. Am. Chem. Soc.* **2005**, *127*, 14558–14559.

(12) Moan, J.; Berg, K. *Photochem. Photobiol.* **1991**, *53*, 549–553.

(13) Scandola, F.; Chiorboli, C.; Prodi, A.; Iengo, E.; Alessio, E. *Coord. Chem. Rev.* **2006**, *250*, 1471–1496.

(14) Schöder, H. *Nuclear Oncology*; Springer: New York, 2013; pp 269–295.

(15) (a) Biel, M. A. *Photodynamic Therapy*; Springer: New York, 2010; pp 281–293. (b) Vesper, B. J.; Colvard, M. D., *Head & Neck Cancer: Current Perspectives, Advances, and Challenges*; Springer: New York, 2013; pp 649–676.

(16) Henderson, B. W.; Waldow, S. M.; Potter, W. R.; Dougherty, T. J. *Cancer Res.* **1985**, *45*, 6071–6077.